ORIGINAL RESEARCH

Augmentation of Endothelial S1PR1 Attenuates Postviral Pulmonary Fibrosis

Patricia L. Brazee[1], Andreane Cartier[3], Andrew Kuo[3], Alexis M. Haring[1], Trong Nguyen[1], Lida P. Hariri[2], Jason W. Griffith[1], Timothy Hla[3], Benjamin D. Medoff[1]*, and Rachel S. Knipe[1]*

[1]Center for Immunology and Inflammatory Diseases, Division of Pulmonary and Critical Care, [2]Department of Pathology, Massachusetts General Hospital, and [3]Vascular Biology Program, Department of Surgery, Boston Children's Hospital, Harvard Medical School, Boston, Massachusetts

Abstract

Respiratory viral infections are frequent causes of acute respiratory distress syndrome (ARDS), a disabling condition with a mortality of up to 46%. The pulmonary endothelium plays an important role in the development of ARDS as well as the pathogenesis of pulmonary fibrosis; however, the therapeutic potential to modulate endothelium-dependent signaling to prevent deleterious consequences has not been well explored. Here, we used a clinically relevant influenza A virus infection model, endothelial cell–specific transgenic gain-of-function and loss-of-function mice as well as pharmacologic approaches and *in vitro* modeling, to define the mechanism by which S1PR1 expression is dampened during influenza virus infection and determine whether therapeutic augmentation of S1PR1 has the potential to reduce long-term postviral fibrotic complications. We found that the influenza virus–induced inflammatory milieu promoted internalization of S1PR1, which was pharmacologically inhibited with paroxetine, an inhibitor of GRK2. Moreover, genetic overexpression or administration of paroxetine days after influenza virus infection was sufficient to reduce postviral pulmonary fibrosis. Taken together, our data suggest that endothelial S1PR1 signaling provides critical protection against long-term fibrotic complications after pulmonary viral infection. These findings support the development of antifibrotic strategies that augment S1PR1 expression in virus-induced ARDS to improve long-term patient outcomes.

Keywords: influenza virus; endothelium; sphingosine 1 phosphate receptor 1; fibrosis

Acute respiratory distress syndrome (ARDS) is a disabling condition with a mortality of up to 46%. Pulmonary infections are common causes of ARDS, with respiratory viral infections such as influenza and coronaviruses being some of the more frequent infectious etiologies (1, 2). Interestingly, data from patients with ARDS has shown a strong association between viral infection and the development of post-ARDS fibrosis (3–5). Although supportive interventions have reduced the overall mortality of ARDS, severe cases requiring prolonged mechanical ventilation remain common and are often characterized by excessive fibroproliferation in the lung, reduced quality of life, and increased mortality (5–10). Consistent with human data, influenza A virus (IAV) infection in mice has been shown to result in long-term lung fibrosis (9, 11). Thus, with the predominance of respiratory viral infections, there is a critical need to understand the mechanisms behind postviral fibrosis and develop novel therapeutic strategies to avoid this morbid complication.

Under homeostatic conditions, the pulmonary endothelium forms a cellular

(Received in original form August 3, 2023; accepted in final form November 7, 2023)

*Co–last authors.

Supported by National Heart, Lung, and Blood Institute Division of Intramural Research grants HL116275, HL133153, HL135821, HL140175, HL147059, HL157384, and HL168138 and by Division of Intramural Research, National Institute of Allergy and Infectious Diseases, grant AI173377.

Author Contributions: Conceptualization: P.L.B., B.D.M., and R.S.K. Methodology: P.L.B., J.W.G., T.H., B.D.M., and R.S.K. Formal analysis: P.L.B. Investigation: P.L.B., A.C., A.K. A.M.H., and T.N. Resources: J.W.G., L.P.H., and T.H. Writing – original draft: P.L.B., B.D.M., and R.S.K. Writing – review and editing: P.L.B., J.W.G., T.H., B.D.M., and R.S.K. Visualization: P.L.B. Supervision: P.L.B., T.H., B.D.M., and R.S.K. Funding acquisition: P.L.B., B.D.M., and R.S.K.

Correspondence and requests for reprints should be addressed to Rachel S. Knipe, M.D., Center for Immunology and Inflammatory Diseases, Division of Pulmonary and Critical Care, Massachusetts General Hospital, Harvard Medical School, Bulfinch 148, 55 Fruit Street, Boston, MA 02114. E-mail: rknipe@mgh.harvard.edu.

This article has a related editorial.

This article has a data supplement, which is accessible from this issue's table of contents at www.atsjournals.org.

Am J Respir Cell Mol Biol Vol 70, Iss 2, pp 119–128, February 2024

Originally Published in Press as DOI: 10.1165/rcmb.2023-0286OC on November 7, 2023
Internet address: www.atsjournals.org

Clinical Relevance

Our study provides evidence that therapeutic augmentation of S1PR1, a key protective signaling axis for the lung endothelium, has the potential to reduce postviral fibrosis. These findings, which mechanistically characterize the regulation of endothelial S1PR1 signaling in postviral pulmonary fibrosis, address the urgent need for therapies targeted at reducing endothelial cell dysfunction and reducing long-term postviral fibrotic complications in acute respiratory distress syndrome survivors.

barrier that separates the vascular compartment from the surrounding lung parenchyma. The effectiveness of this barrier is determined by the functionality of endothelial cells (ECs) and the integrity of the intercellular junctions between them. Injury to the epithelial layer that occurs during respiratory viral infection exposes the closely associated pulmonary endothelium to the pathological inflammatory milieu, resulting in EC injury and activation, a central component of ARDS pathophysiology (6–9). Activated ECs assume a proinflammatory phenotype that amplifies lung injury and increases vascular permeability (12, 13). Although increased barrier permeability facilitates immune-mediated viral clearance before tissue repair, persistent EC activation with vascular leak has pathologic consequences, including the generation and flux of proinflammatory, procoagulant, and profibrotic mediators (5, 14–22). Currently, there are limited therapies to reduce vascular leak, and, in fact, supportive mechanical ventilation may further exacerbate this pathological endothelial injury (22). A better understanding of the molecular mechanisms that promote EC dysfunction in ARDS and the effects on subsequent fibrosis could lead to novel therapeutic strategies.

The sphingosine-1-phosphate (S1P)–S1P receptor 1 (S1PR1) signaling axis on ECs is a key modulator of vascular permeability, cell survival, and inflammation (23, 24). Notably, we have previously defined a causal link between vascular leak and pulmonary fibrosis, showing that the endothelium-specific deletion of S1PR1 results in increased vascular leak and pulmonary fibrosis in a mouse model of bleomycin-induced lung injury and fibrosis (14, 24). Although preventative agonism of S1PR1 has been shown to reduce acute IAV-induced inflammation and increase survival (16), the role of S1PR1 during the fibroproliferative phase of pulmonary viral infection–induced ARDS has not been well explored. Reversing endothelial dysfunction and restoring pulmonary vascular integrity via augmentation of endothelial S1PR1 in virus-induced ARDS could have great therapeutic value.

Our data demonstrate that both murine and human IAV infection is associated with loss of EC S1PR1 that correlates with injury severity and collagen deposition. Using EC S1PR1 gain-of-function and loss-of-function mice in an IAV infection model, we found that loss of endothelial S1PR1 is deleterious, with enhanced vascular leak and pulmonary fibrosis, whereas EC-specific S1PR1 overexpression reduces vascular leak and postviral fibrosis. Our data suggest that inflammation-induced elevation of S1P drives a maladaptive, persistent internalization of EC S1PR1. Moreover, we show that genetic and pharmacologic augmentation of S1PR1 after IAV infection is sufficient to reduce postviral fibrosis. Taken together, our findings support the development of antifibrotic strategies that augment EC S1PR1, potentially via GRK2 inhibition, to reduce the burden of postviral fibrosis.

Methods

Mice

Wild-type (WT) C57BL/6 mice were purchased from Charles River Laboratories. Mice with the *S1pr1* gene flanked by loxP sites (*S1pr1*$^{f/f}$) were provided by Dr. Jerold Chun (25). S1pr1$^{f/STOP/f}$ mice, provided by T.H., carry a conditional *S1pr1* expression cassette with a loxP-flanked STOP cassette that prevents transcription of S1pr1 until Cre recombinase–mediated excision of the floxed STOP cassette, which promotes overexpression of *S1pr1* (26). Each line was crossed with mice that express an inducible Cre recombinase under an EC-specific promoter (VECadherin^{CreERT2}), shared by Dr. Ralf Adams (27). All mice were on a C57BL/6 background. Littermates with corresponding loxP sites but lacking the VECadherin^{CreERT2} gene were used as control animals (EC_{norm}). Mice were treated with 200 mg/kg tamoxifen (Sigma-Aldrich, catalog no. T5648) by oral gavage for 2 weeks (10 doses, Monday to Friday) beginning at age 4 weeks. For postviral induction of Cre activity, mice were treated with 200 mg/kg tamoxifen by oral gavage for 1 week (five doses, Monday to Friday) beginning at 7 days postinfection (age 10–12 wk). The efficiency of tamoxifen induction of Cre recombinase–mediated deletion in S1pr1$^{f/f}$VECadherin^{CreERT2} mice (*see* Figure E3A in the data supplement) and overexpression before IAV infection (Figure E4A) and after infection (Figure E4Q) in S1pr1$^{f/STOP/f}$VECadherin^{CreERT2} mice were monitored by quantification of S1PR1.

All mice were maintained in a specific pathogen–free environment certified by the American Association for Accreditation of Laboratory Animal Care. All protocols performed were approved by the Massachusetts General Hospital Institutional Animal Care and Use Committee. All experiments used sex-matched male and female mice at 10 to 12 weeks of age.

IAV Infection and Viral Quantification

The influenza A/Puerto Rico/8/34 (PR8) H1N1 strain was obtained from Charles River Laboratories (catalog no. 10100374). Mice were anesthetized with ketamine (80 mg/kg)-xylazine (12 mg/kg) and intranasally infected with a dose of influenza PR8 that leads to ∼15% mortality (lethal dose 15; 100 egg infectious dose /g) at 10–12 weeks of age. Uninfected mice received anesthesia as noted above and are denoted as "0 dpi" (0 d postinfection), indicative of a state without exposure to influenza virus. Viral titers were determined by quantification of viral transcripts using qRT-PCR as previously described and outlined below (28–31).

qRT-PCR

RNA was converted to cDNA (QuantaBio, catalog no. 95047), and qPCRs in the presence of SYBR Green (Bio-Rad Laboratories, catalog no. 1725271) were performed using the primers listed below.

IAV polymerase (PA), 5′-CGGTCCAA ATTCCTGCTGA-3′ (forward) and 5′-CAT TGGGTTCCTTCCATCCA-3′(reverse); IAV nucleoprotein (NP), 5′-CAGCCTAAT

CAGACCAAATG-3′ (forward) and 5′-TAC CTGCTTCTCAGTTCAAG-3′ (reverse); IAV hemagglutinin (HA), 5′-GAGGAG CTGAGGGAGCAAT-3′ (forward) and 5′-GCCGTTACTCCGTTTGTGTT-3′ (reverse); mouse *Gapdh*, 5′-AGGTCGGTGT GAACGGATTTG-3′ (forward) and 5′-TGT AGACCATGTAGTTGAGGTCA-3′; mouse *S1pr1*, 5′-ATGGTGTCCACTAGCATCCC-3′ (forward) and 5′-CGATGTTCAACTTG CCTGTGTAG-3′ (reverse), mouse *Sphk1*, 5′-ACTGATACTCACCGAACGGAA-3′ (forward) and 5′-CCATCACCGGACA TGACTGC-3′ (reverse); mouse *Grk2*, 5′-GCGCCAGCAAGAAGATCCT-3′ (forward) and 5′-GCAGAAGTCCCGGAAAA GCA-3′ (reverse); human *S1PR1*, 5′-TCTG CTGGCAAATTCAAGCGA-3′ (forward) and 5′-GTTGTCCCCTTCGTCTTTCTG-3′ (reverse); human *SPHK1*, 5′-GGCTGCTG TCACCCATGAA-3′ (forward) and 5′-TCA CTCTCTAGGTCCACATCAG-3′ (reverse); human *GAPDH*, 5′-ACAACTTTGGTATC GTGGAAGG-3′ (forward) and 5′-GCCATC ACGCCACAGTTTC-3′ (reverse); human *EDNRA*, 5′-TCGGGTTCTATTTCTGTAT GCCC-3′ (forward) and 5′-TGTTTTTGCC ACTTCTCGACG-3′ (reverse); human *EDNRB*, 5′-GTCCCAATATCTTGATCGC CAG-3′ (forward) and 5′-AAGGCACC AGCTTACACATCT-3′ (reverse); human EDN1, 5′-AGAGTGTGTCTACTTCTGC CA-3′ (forward) and 5′-CTTCCAA GTCCATACG GAACAA-3′ (reverse); human *CTHCR1*, 5′-CAATGGCATTCCG GGTACAC-3′ (forward) and 5′-GTACA CTCCGCAATTTTC CCAA-3′ (reverse).

BAL

BAL fluid (BALF) was collected as previously described (32). Total protein was quantified by bicinchoninic acid assay (Thermo Scientific, catalog no. 23225).

Hydroxyproline Assay

Left lung lobes were extracted and processed for hydroxyproline quantification as previously described (14).

Flow Cytometry

At the time of harvest, mice were administered CD45.2-AF700 (BioLegend, catalog no. 109822) retroorbitally to stain circulating cells (IV-CD45). Single-cell suspensions of lung were stained as follows. Samples were blocked with purified CD16/CD32 mAb (BD Biosciences, catalog no. 553142) and then stained with fluorescently labeled surface antibodies. Endothelial cocktail included CD45-FITC (BioLegend, catalog no. 103018), CD31-PE-Cy7 (BioLegend, catalog no. 102418), EpCAM-BV605 (BioLegend, catalog no. 118227), and S1PR1-APC (R&D Systems, catalog no. FAB7089A). Myeloid cocktail included MHCII-BV510 (BioLegend, catalog no. 107635), F4/80-BV421 (BioLegend, catalog no. 123137), CD64-BV605 (BioLegend, catalog no. 139323), Ly6G-AF488 (BioLegend, catalog no. 127626), CD11c-PE-Cy7 (BioLegend, catalog no. 117318), Siglec F-PE (BD Biosciences, catalog no. 552126), CD11b-APC (BioLegend, catalog no. 101212), and Ly6C-PerCP-Cy5.5 (BioLegend, catalog no. 128012). The T cell panel included TCRβ-BV610 (BioLegend, catalog no. 109241), CD4-BV785 (BioLegend, catalog no. 100453), CD3-BV421 (BioLegend, catalog no. 100335), CD44-BV510 (BioLegend, catalog no. 103043), CD8-PE-Cy7 (BioLegend, catalog no. 100722), and TCRγδ-PerCP-Cy5.5 (Invitrogen, catalog no. 46-5711-82). Viability staining (e780, Invitrogen, 65-0865-14) was done at room temperature for 15 minutes in all panels. Cells were fixed in 4% paraformaldehyde (BioLegend, catalog no. 420801) for 20 minutes at room temperature. Intracellular staining for FOXP3-AF488 (Invitrogen, catalog no. 53-5773-82) was performed using the True-Nuclear Transcription Factor Buffer Set (BioLegend, catalog no. 424401) according to the manufacturer's instructions. Flow cytometry was performed on a Beckman Coulter CytoFLEX 5 flow cytometer and analyzed using FlowJo (version 10.8.1). After exclusions of doublets, dead cells, and IV-$CD45^+$ cells, populations were gated and defined as previously described and as outlined in Figures E1A–E1C (32).

Western Blot

Tissue and cell lysis was performed as previously described (14). Primary antibodies used were as follows: S1PR1 (ABclonal, catalog no. A12935, 1:1000) and GAPDH (Cell Signaling Technology, catalog no. 2118, 1:1,000). The fluorescently labeled secondary antibody used was goat anti-rabbit (LI-COR Biosciences, catalog no. 926-32211, 1:10,000). Blots were visualized on a LI-COR Odyssey CLx instrument.

Histopathology

Mice were killed at Day 0, 7, 14, 21, or 42 after infection. Lung lobes were inflated with 4% paraformaldehyde (Fisher, catalog no. 50-980-487) and then placed in cold paraformaldehyde for 15 minutes before transfer to cold PBS. Paraffin-embedded 5-μm sections were stained with hematoxylin and eosin or Masson's trichrome stain. Bright-field images were obtained using a Zeiss Axioscan Z1 slide scanner microscope. Lung severity and Ashcroft scores were assessed as previously described (32, 33).

Optimal cutting temperature (O.C.T.)-embedded cryosections were stained for S1PR1 (Santa Cruz Biotechnology, catalog no. H60), VECAD (R&D Systems, catalog no. AF1002), and DAPI (Thermo Fisher Scientific, catalog no. D1306). Confocal images were taken using an Olympus FluoView FV10i or Zeiss LSM 3 800 with Airyscan microscopes.

Human Tissue

Lung tissue was obtained from human autopsy under an institutional review board approval. Specimens were retrospectively evaluated by a pathologist to identify "moderate injury" specimens from three individuals infected with IAV. Paraffin-embedded 5-μm sections were stained and imaged as described above. Individual lung sections were subclassified into mild (score 1–2), moderate (score 2–3), and severe (score 3–4) areas across each tissue slice.

S1P Measurements

S1P was quantified by liquid chromatography tandem mass spectrometry using an LCMS-8050 system (triple quadrupole; Shimadzu) as described (34).

Cell Lines

Human lung microvascular endothelial cells (HLMVECs) were purchased from Lonza (catalog no. CC-2527) and cultured according to the manufacturer's instructions. All cells were grown in a humidified incubator with 5% CO_2 at 37°C and routinely tested for mycoplasma contamination.

Other Reagents

HLMVECs were treated with the following pooled siRNA (60 pmol) purchased from Santa Cruz Biotechnology: siS1PR1-h (SC-37086), siSPHK1-h (SC-44114), and siControl-A (SC-37007). siRNA was used complexed with RNAiMAX (Thermo Fisher Scientific, catalog no. 13778). HLMVECs were treated for 16 hours with the following recombinant human cytokines purchased from BioLegend and used at 5 ng/ml: IL-6

(catalog no. 570802), IFN-α (catalog no. 592702), TNF-α (catalog no. 570102), and IL-1α (catalog no. 570002). The inflammatory cocktail (IC) was composed of equal parts IL-6, IFN-α, TNF-α, and IL-1α, each at 5 ng/ml. For *in vitro* experiments, FTY720 (10 nM, catalog no. SML0700-5MG) and paroxetine hydrochloride (Px; 25 μM, catalog no. P9623-10 mg) were purchased from Sigma-Aldrich. For *in vivo* experiments, Px (catalog no. 14998) was purchased from Cayman Chemical and given by daily intraperitoneal injection (20 mg/kg body weight/d) (35–37). We observed no toxicity or mortality in uninfected vehicle or Px-treated mice (data not shown).

Statistical Analysis

Analyses of significance were performed using GraphPad Prism (version 9.1.1) software. A *P* value less than or equal to 0.05 was considered statistically significant. A standard two-tailed unpaired Student's *t* test was used for two groups. One-way ANOVA, followed by analysis-specific posttests, was performed when more than two groups were compared. Two-way ANOVA was used with two or more groups with two variables. Data are presented as mean ± SD overlaid with individual data points representing replicates. Statistical analysis of survival curves was performed with a two-sided log-rank (Mantel-Cox) test.

Results

Loss of Endothelial S1PR1 Correlates to Degree of Post-Viral Fibrosis

Immunofluorescent costaining of lung specimens from IAV-infected patients for endothelial specific marker VE-cadherin (VECad) and S1PR1 suggested colocalization in areas of mild injury, with loss of S1PR1 in moderate and severe areas (Figure 1A). Masson's trichrome staining revealed more evident parenchymal deposition of collagen in more severely injured lung regions (Figure 1B). These observations suggest a putative inverse relationship between lung injury and collagen deposition with the expression of endothelial S1PR1 in human IAV infection.

To define the possible association between reduced endothelial S1PR1 and increased deposition of collagen, we used a low-dose IAV infection model in WT mice with significant weight loss and low mortality (Figures E2A and E2B). Viral titers were significantly elevated at 7 days postinfection (dpi) with no significant signal by 14 dpi (Figures E2C–E2E). Total protein in BALF was used to quantify vascular leak as a proxy for lung injury in our model (14, 38). BALF total protein was increased at 7 dpi, peaked at 14 dpi, and remained elevated at 21 dpi, returning to baseline by 42 dpi (Figure E2F). Consistent with observations in human specimens, immunofluorescence showed VECad and S1PR1 costaining at 0 dpi that was absent at later time points (Figure 2A). Masson's trichrome stain revealed an inverse pattern, where collagen deposition, absent at 0 dpi, became more evident at 14 dpi and persisted through 21 dpi (Figure 2B). Quantification of lung fibrosis by hydroxyproline (OHP) assay showed increased OHP by 14 dpi that resolved slightly by 21 dpi but remained persistently elevated to 42 dpi (Figure 2C). Quantification of S1PR1 median fluorescence intensity showed reductions in S1PR1 by 7 dpi that continued to decrease at 14 dpi and remained below baseline to 42 dpi (Figure 2D). These quantitative measures of fibrosis and S1PR1 show an inverse relationship between lung fibrosis and endothelial S1PR1 expression (Figure 2E) and suggest that a loss of EC S1PR1 associates with increased post-IAV fibrosis.

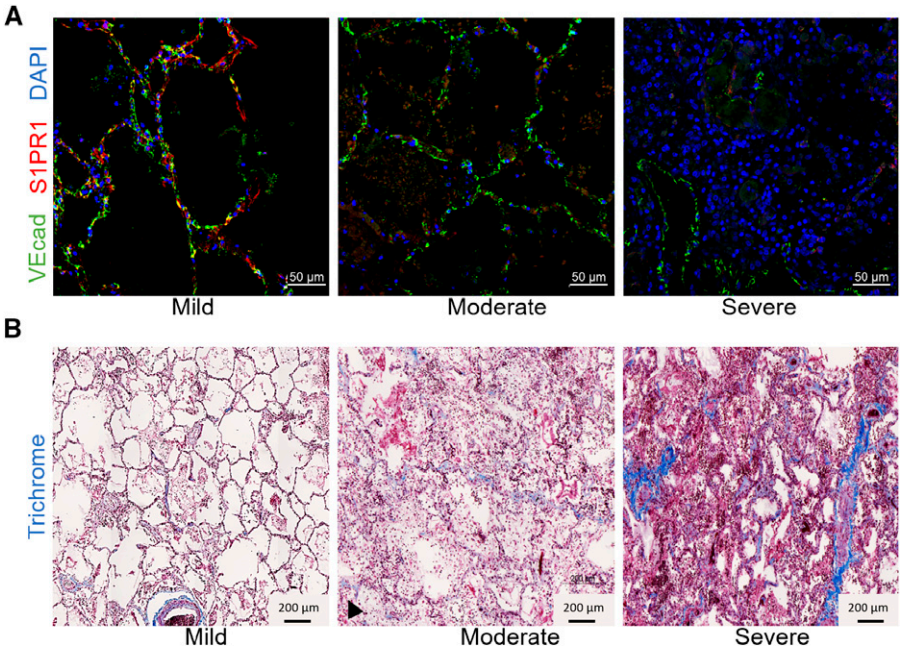

Figure 1. Loss of endothelial S1PR1 associated with collagen deposition in sections of human lung tissue obtained at autopsy of patients with influenza A virus (IAV) infection. (*A*) Immunofluorescent costaining of DAPI (blue), VE-cadherin (green), and S1PR1 (red) in representative mild, moderate, and severely affected areas. $n = 3$ patients. Scale bars, 50 μm. (*B*) Brightfield Masson's trichrome stain showing collagen deposition (blue) in representative mild, moderate, and severely affected areas. $n = 3$ patients. Scale bars, 200 μm.

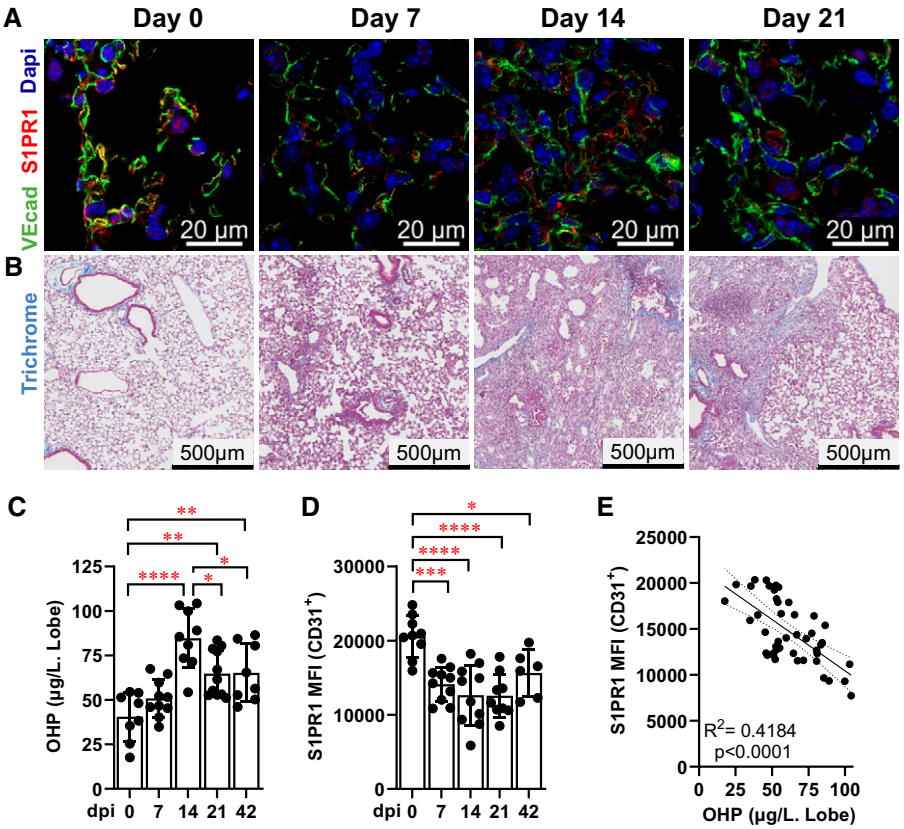

Figure 2. Loss of endothelial S1PR1 correlates with the degree of fibrosis in a mouse model of IAV infection. (*A*) Immunofluorescent costaining of DAPI (blue), VE-cadherin (green), and S1PR1 (red) ($n = 3$ mice per time point). Scale bars, 20 μm. (*B*) Brightfield Masson's trichrome stain showing collagen deposition (blue) ($n = 3$ mice per time point). Scale bars, 500 μm. (*C*) Fibrosis as measured by hydroxyproline (OHP) content of left lung lobe. (*D*) FACS quantification of median fluorescence intensity (MFI) of S1PR1 stain on $CD45^{-}EpCAM^{-}CD31^{+}$ cells. (*E*) Linear correlation between OHP levels and endothelial cell (EC) S1PR1 MFI across all time points in IAV-infected mice. (*C* and *D*) Mean ± SD overlaid with individual data points, each representing one mouse from three independent experiments. $^{*}P < 0.05$, $^{**}P < 0.01$, $^{***}P < 0.005$, $^{****}P < 0.0001$ (one-way ANOVA, Bonferroni *post hoc* test). dpi = days postinfection; OHP = hydroxyproline.

Endothelium-Specific Modulation of S1PR1 Determines Degree of Postviral Fibrosis

To address the causal role of EC S1PR1 in postviral fibrosis, we used loss-of-function transgenic mice to 21 dpi, where we see persistent fibrosis in our model. Mice with an inducible endothelium-specific deletion of S1PR1 ($S1pr1^{f/f}$ $VECad^{CreERT2}$, EC_{ko}) (14, 26) displayed persistent loss of EC S1PR1 expression (Figure E3A), with increased mortality compared with EC_{norm} ($S1pr1^{f/f}$) littermates (Figure 3A). We did not observe differences in viral clearance (Figures E3B–E3D) between EC_{ko} and EC_{norm} mice.

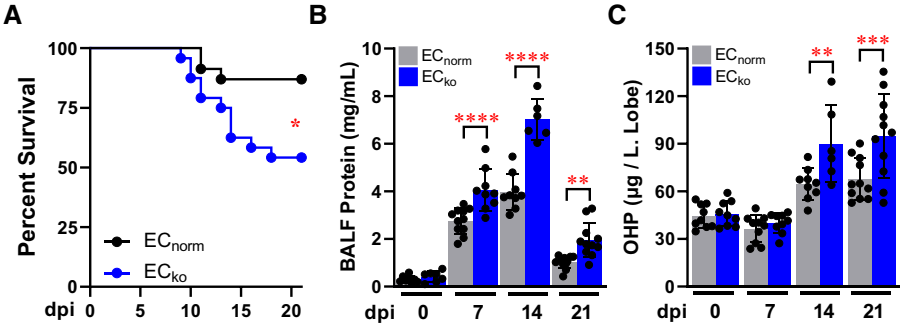

Figure 3. Endothelial deletion of S1PR1 leads to poor outcomes in IAV infection model. (*A*) Percentage survival ($n = 23$ mice per group). (*B*) Total protein content in BAL fluid (BALF). (*C*) Quantification of OHP content of left lung lobe. (*B* and *C*) Mean ± SD overlaid with individual data points, each representing one mouse from three independent experiments. $^{*}P < 0.05$, $^{**}P < 0.01$, $^{***}P < 0.005$, $^{****}P < 0.0001$ (*B* and *C*, two-way ANOVA, Bonferroni *post hoc* test; *A*, two-tailed log-rank Mantel-Cox test).

Flow cytometry of lung single-cell suspensions revealed elevated numbers of $MHCII^{lo}CD11b^{+}Ly6C^{+}CD64^{+}$ monocytes (Figure E3E), $Ly6G^{+}$ neutrophils (Figure E3F), and $MHCII^{hi}CD11c^{hi}$ dendritic cells (Figure E3G) in EC_{ko} compared with EC_{norm} mice at 7 dpi. By 14 dpi, no differences were observed in these populations. Differences were not observed in $SiglecF^{+}CD11b^{low}$ alveolar macrophages, $MHCII^{high}CD11b^{+}F4/80^{+}CD64^{+}$ macrophages, $TCR\gamma\delta^{+}$ T cells, $TCR\beta^{+}CD4^{+}CD44^{+}CD69^{+}$ T cells, $TCR\beta^{+}CD4^{+}Foxp3^{+}CD44^{+}CD69^{+}$ regulatory T cells, or $TCR\beta^{+}CD8^{+}CD44^{+}CD69^{+}$ T cells between EC_{ko} and EC_{norm} (Figures E3H–E3M). However, we detected elevated BALF total protein levels in EC_{ko} mice compared with EC_{norm} littermates at 7, 14, and 21 dpi (Figure 3B). Examination of hematoxylin and eosin–stained lung sections showed increased severity of lung injury in EC_{ko} at 21 dpi compared with EC_{norm} littermates (Figure E3N). We observed elevated OHP levels at 14 and 21 dpi in EC_{ko} mice compared with EC_{norm} littermates (Figure 3C), consistent with increased Ashcroft scoring of trichrome-stained lung sections at 21 dpi (Figure E3O). These results suggest a mechanistic link between loss of EC S1PR1 and postviral fibrosis.

Gain-of-function transgenic mice ($S1pr1^{f/STOP/f}$ $VECad^{CreERT2}$, EC_{high}) (26) were used to determine if overexpression of EC S1PR1 was sufficient to protect against post-IAV fibrosis. Overexpression of S1PR1 was not sufficient to prevent IAV infection–associated decreases in EC S1PR1, but levels did remain elevated at all time points compared with EC_{norm} littermates ($S1pr1^{f/STOP/f}$, EC_{norm}) (Figure E4A). Notably, EC S1PR1 expression in EC_{high} mice increased from 14 to 21 dpi, whereas EC_{norm} littermates had persistent loss of EC surface S1PR1 expression. We observed improved survival (Figure 4A), with no differences in viral clearance compared with EC_{norm} littermates (Figures E4B–E4D). With the exception of moderately reduced neutrophil recruitment in EC_{high} mice compared with EC_{norm} littermates (Figure E4E), we observed no differences in immune cell recruitment between EC_{high} and EC_{norm} mice (Figures E4F–E4M). BALF total protein was decreased in EC_{high} mice compared with EC_{norm} littermates at 14 dpi and normalized by 21 dpi (Figure 4B). Hematoxylin and eosin–stained sections showed reduced severity of lung injury in EC_{high} at 21 dpi compared with EC_{norm} littermates (Figure E4N). We measured reduced OHP levels in EC_{high} mice compared with EC_{norm} littermates at 14 and 21 dpi (Figure 4C), consistent with reduced Ashcroft scores of trichrome staining at 21 dpi (Figure E4O). These results suggest that enhanced EC S1PR1 expression is sufficient to attenuate postviral fibrosis.

To determine whether therapeutic restoration of EC S1PR1 was sufficient to improve outcomes after IAV infection, we took advantage of our inducible system to promote EC S1PR1 overexpression starting at 7 dpi (Figure 4D), when we began to observe clinical symptoms, including weight loss and lung injury, but before appreciable fibrosis. This regimen was sufficient to induce S1PR1 overexpression compared with EC_{norm} littermates (Figure E4P). Although we did not observe a difference in survival (Figure 4E), therapeutic overexpression of EC S1PR1 attenuated the development of fibrosis in EC_{high} mice compared with EC_{norm} littermates (Figure 4F). Taken together, our results demonstrate that

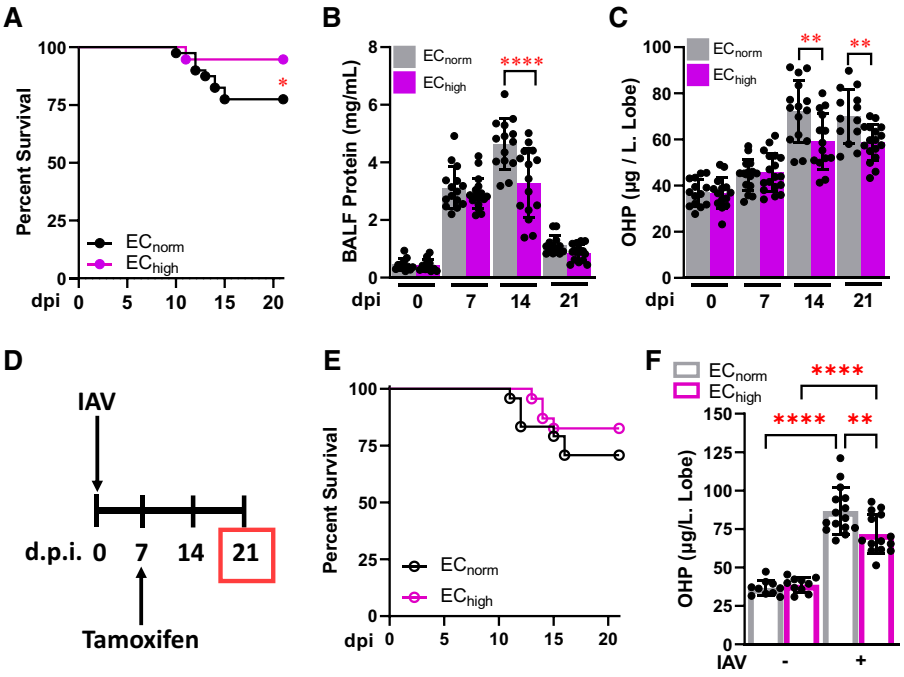

Figure 4. Endothelial overexpression can be employed therapeutically to reduce fibroproliferation in a mouse model of IAV infection. (*A–C*) Overexpression induced before IAV infection. (*D–F*) Tamoxifen to induce therapeutic overexpression begun at 7 dpi. (*A* and *E*) Percentage survival (*A*, $n = 37$ mice per group; *E*, $n = 23$ mice per group). (*B*) Total protein content in BALF. (*C* and *F*) Quantification of OHP content of left lung lobe. (*B*, *C*, and *F*) Mean ± SD overlaid with individual data points, each representing one mouse from three independent experiments. $^{*}P < 0.05$, $^{**}P < 0.01$, $^{****}P < 0.0001$ (*B*, *C*, and *F*, two-way ANOVA, Bonferroni *post hoc* test; *A* and *E*, two-tailed log-rank Mantel-Cox test).

rebound of EC surface S1PR1 expression dampens postviral pulmonary fibrosis.

IAV-induced Inflammation Promotes EC S1PR1 Internalization

To better understand EC S1PR1 regulation during IAV infection, we quantified *S1PR1* mRNA from sorted CD31$^+$ ECs and observed no changes (Figure 5A). Western blotting of whole-lung homogenates from WT mice revealed loss of total S1PR1 (Figure 5B). To recapitulate the *in vivo* inflammatory IAV infection milieu and determine whether a secreted factor upregulated during IAV infection was sufficient to trigger reduced EC S1PR1 expression, we exposed HLMVECs to BALF from WT mice at 0 and 14 dpi *in vitro*. Consistent with *in vivo* findings, we observed reduced S1PR1 protein expression (Figure 5C) without mRNA changes (Figure 5D). To parse whether a specific cytokine was driving this response or if this was a more general consequence of inflammation, HLMVECs were treated with a subset of inflammatory cytokines upregulated during IAV infection (TNF-α, IL-1α, IL-6, and IFN-α), as well as with an IC, composed of each of the tested cytokines. Interestingly, each was sufficient to reduce S1PR1 surface expression with no additive effect from the IC (Figure E5A). Taken together, these data suggest that IAV-associated inflammation is sufficient to trigger post-transcriptional loss of EC S1PR1.

Upon receptor ligation, S1PR1 is phosphorylated by G protein–coupled receptor kinase 2 (GRK2) and is then internalized via a β-arrestin–dependent mechanism. From there, S1PR1 can be recycled back to the cell surface or ubiquitinated by WWP2 and degraded by the proteasome (23, 39). Studies using the S1PR functional antagonist FTY720 have shown that exuberant S1PR1 signaling skews the system toward internalization with subsequent degradation (23, 40, 41). Correspondingly, we detected significantly elevated levels of the endogenous S1PR1 ligand, S1P, in the serum of IAV-infected mice at 14 dpi (Figure E5B), when we first observed a reduction in total cell levels of S1PR1 (Figure 5B). It has been documented that TNF-α and IL-1α can increase the expression and activity of sphingosine kinase 1 (SPHK1), one of the kinases that phosphorylates sphingosine to generate S1P (42). Linking elevated S1P levels to IAV-induced inflammation, we detected upregulation of *Sphk1* in sorted CD31$^+$ ECs (Figure 5E) and enhanced *SPHK1* mRNA in IC-treated HLMVECs (Figure E5C). To

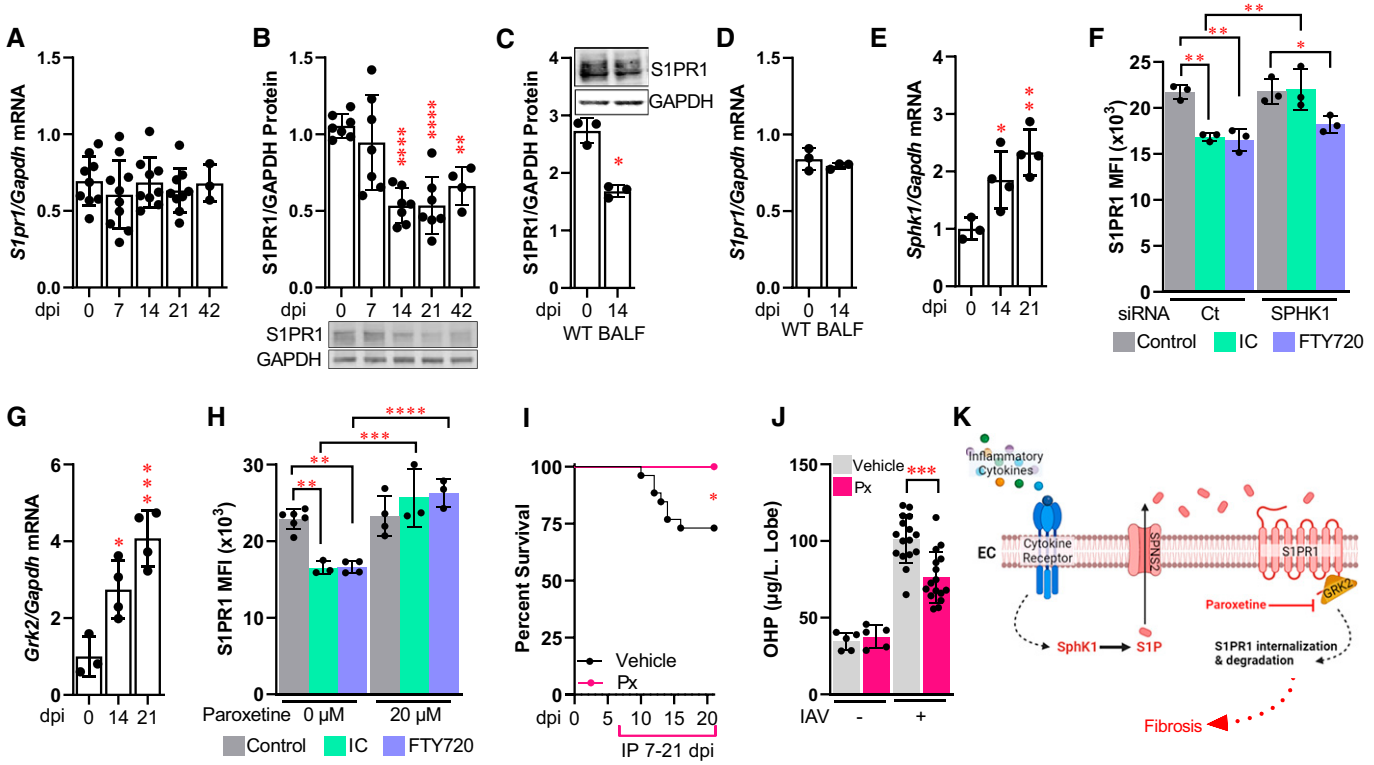

Figure 5. Inhibition of GRK2 is sufficient to restore S1PR1 expression and reduce postviral fibrosis. (*A*) qRT-PCR quantification of *S1pr1/Gapdh* expression in sorted CD31$^+$ ECs at time points after IAV infection. (*B*) Representative Western blot and relative quantification of S1PR1 expression in mouse whole-lung homogenates at time points after IAV infection. (*C*) Representative Western blot and relative quantification of S1PR1 expression in human lung microvascular endothelial cells (HLMVECs) treated with BALF from mice at 0 and 14 dpi. (*D*) qRT-PCR quantification of *S1pr1/Gapdh* expression in HLMVECs treated with BALF from mice at 0 and 14 dpi. (*E*) qRT-PCR quantification of *Sphk1/Gapdh* expression in sorted CD31$^+$ ECs at time points after IAV infection. (*F*) S1PR1 MFI of HLMVECs (siControl [Ct] or siSphk1) treated with inflammatory cocktail (IC) or FTY720. (*G*) qRT-PCR quantification of *Grk2/Gapdh* expression in sorted CD31$^+$ ECs at time points after IAV infection. (*H*) S1PR1 MFI of HLMVECs treated with IC or FTY720 with and without paroxetine. (*I*) Survival proportions of IAV-infected mice that received paroxetine or vehicle treatment. (*J*) Quantification of OHP content of left lung lobe. (*K*) Schematic of S1PR1 regulation during IAV infection. Mean ± SD overlaid with individual data points representing replicates. *$P<0.05$, **$P<0.01$, ***$P<0.005$, ****$P<0.0001$ (*A*, *B*, *E*, and *G*, one-way ANOVA, Bonferroni *post hoc* test; *C* and *D*, two-tailed *t* test; *F*, *H*, and *J*, two-way ANOVA Bonferroni *post hoc* test; *I*, two-tailed log-rank Mantel-Cox test).

determine if SPHK1 was necessary to induce loss of S1PR1, HLMVECs transfected with either a control siRNA or siRNA targeting *SPHK1* were treated with IC or FTY720. With silencing of *SPHK1*, surface levels of S1PR1 were resistant to inflammation-mediated internalization (Figure 5F). However, because FTY720 directly binds to S1PR1 and does not require endogenous S1P production, silencing of *SPHK1* was not sufficient to rescue FTY720-mediated S1PR1 internalization (Figure 5F). Collectively, these results show that inflammatory activation of SPHK1 is necessary to drive paracrine and/or autocrine S1P-mediated internalization of S1PR1.

Given the pleiotropic effects of S1P, targeting this bioactive lipid directly or via inhibition of SPHK1 is difficult to translate for clinical relevance (43). As such, we probed the internalization pathway downstream of S1PR1 ligation for therapeutic targets. In sorted $CD31^+$ ECs, we detected elevated expression of *Grk2* (Figure 5G), the kinase that phosphorylates S1PR1 to trigger its internalization (42). Using Px, a U.S. Food and Drug Administration–approved selective serotonin reuptake inhibitor that has been shown to inhibit GRK2 and impede the internalization of S1PR1 (39, 44, 45), we were able to rescue both IC and FTY720-induced reductions in surface S1PR1 (Figure 5H). We next tested the efficacy of Px *in vivo* to improve outcomes and attenuate postviral lung fibrosis. Naive and IAV-infected mice received daily Px starting at 7 dpi. IAV-infected mice receiving Px had increased survival compared with vehicle-treated littermates (Figure 5I). At 21 dpi, both groups developed measurable fibrosis compared with uninfected mice; however, OHP content was attenuated in the Px-treated group (Figure 5J), and we observed elevated S1PR1 expression in IAV-infected Px-treated mice compared with vehicle (Figure E5D). Taken together, these data elucidate a mechanism by which IAV-induced inflammation activates SPHK1 to elevate S1P and drive maladaptive internalization of S1PR1 driven by GRK2 that can be inhibited by Px to reduce postviral lung fibrosis (Figure 5K).

Discussion

A substantial proportion of ARDS survivors experience reduced quality of life because of the development of fibrotic changes in the lung (6–10). The pulmonary endothelium has largely been excluded in the study of post-ARDS fibrosis, despite knowledge that EC injury and activation are central components of ARDS pathophysiology (6, 7, 9). Our findings suggest that persistent EC S1PR1 internalization contributes to subsequent downstream sequelae such as lung fibrosis. Because current management of patients with virus-induced ARDS is largely limited to mechanical ventilation, which may further perpetuate pathological endothelial injury, novel therapeutics are urgently needed (22). Our data position EC S1PR1 rebound at the inflection point between normal repair and fibrosis and identify a targetable mechanism of regulation to attenuate post-ARDS fibrosis.

EC S1PR1 is a key regulator of vascular integrity, cell survival, and inflammatory processes (14, 16, 42). We have previously shown that EC-specific deletion of S1PR1 increases susceptibility to bleomycin-induced pulmonary fibrosis (14). However, it was unclear whether EC S1PR1 was necessary for limiting the development of fibrosis across etiologies. Our model used a low dose of IAV that resulted in moderate disease with low mortality, which allowed us to focus on the long-term fibrotic complications of IAV infection. Here we were able to achieve enhanced OHP content comparable with our previous studies using a single-injection bleomycin pulmonary fibrosis model (14). We showed that EC_{ko} mice had increased mortality, modest elevation of immune cell recruitment at 7 dpi, elevated BALF total protein, and persistent fibrosis to 21 dpi compared with EC_{norm} littermates. Conversely, studies have shown that preventative agonism of S1PR1 is sufficient to improve outcomes in a short-term mouse model of severe IAV infection (16). We observed similar findings using, for the first time, to our knowledge, an EC-specific overexpression of S1PR1 in an IAV-infection model. EC_{high} mice have reduced mortality, slightly reduced neutrophils, and decreased BALF total protein and fibrosis compared with EC_{norm} littermates. In addition, our inducible system was used to show that therapeutic induction of S1PR1 is sufficient to attenuate the degree of post-IAV fibrosis. However, we did not detect a difference in survival with therapeutic induction of EC S1PR1 at 7 dpi. In our model, we observed that the majority of our mortality events occurred between Days 10 and 15, a time during which the mice experience significant weight loss and had significantly elevated BALF total protein, indicative of severe lung injury and alveolar–capillary barrier permeability, which can lead to respiratory failure and death in the more severely affected mice. The improved survival with reduced fibrosis observed with Cre activation before IAV infection is likely a dual effect of the known role for EC S1PR1 in limiting postviral inflammation and barrier enhancement. Taken together, these observations may suggest that our therapeutic dosing strategy is not sufficient to protect from the acute inflammatory phase of the disease, but rather inhibits hyperactivation of the later fibroproliferative phase of postviral ARDS.

Early downregulation of EC S1PR1 during IAV infection may represent an adaptive process to facilitate immune-mediated viral clearance necessary before tissue repair can occur. However, the persistence of EC S1PR1 downregulation has pathologic consequences (14). One possible mechanism of protection observed with S1PR1 augmentation is through the restoration of the vascular barrier mediated by S1PR1 signaling, which blunts the influx of proinflammatory, procoagulant, and profibrotic mediators (5, 14–22). With the close proximity of the endothelium to the epithelial and mesenchymal compartments, it is likely that parallel, cell-intrinsic, S1PR1-mediated signaling from the endothelium may also play a role in the attenuation of fibrotic outcomes. These findings highlight the importance of EC S1PR1 in supporting productive lung repair and identify a potential therapeutic avenue to attenuate postviral fibrosis and reduce long-term respiratory dysfunction in ARDS survivors.

Although EC S1PR1 has previously been investigated in the context of IAV infection (16), changes in EC S1PR1 expression have not been reported. We observed an association between IAV-induced injury severity, loss of EC S1PR1 expression, and deposition of collagen in both human and mouse lungs. Here, our data suggest a maladaptive dysregulation of endothelial S1PR1 recycling that results in the persistent loss of S1PR1 and promotes postviral fibrosis. We found that during IAV infection, there was an inflammation-induced upregulation of *SPHK1* that was necessary to promote S1PR1 internalization. It has previously been noted that inflammatory mediators are sufficient to upregulate the expression and activity of

SPHK1, the enzyme that generates S1P (46). This upregulation may contribute to the elevated levels of S1P in the serum of IAV-infected mice as observed by us and others (47). Although these data may point toward SPHK1 as an intriguing target, it has been shown that loss of endothelial SPHK1 is deleterious with increased lung injury and fibrosis after bleomycin challenge (43). Moreover, the SPHK1-generated S1P gradient is crucial for lymphocyte recruitment necessary for viral clearance during IAV infection. Therefore, we focused our investigation downstream of the S1P–S1PR1 interaction to identify more viable therapeutic targets.

Upon receptor ligation, S1PR1 is phosphorylated by GRK2, allowing β-arrestin to bind and internalize S1PR1, which can either be recycled back to the cell surface or marked for proteasomal degradation (23, 42). It is this mechanism that attributes functional antagonism to compounds initially thought to have a purely agonist effect (23, 48), further supporting our focus downstream of S1PR1 ligation to identify a viable therapeutic target. In our IAV infection model, we observed increased expression of EC *Grk2* and found that Px, which is known to inhibit GRK2, was sufficient to prevent persistent loss of surface S1PR1. Mice that received therapeutic dosing of Px had improved survival and reduced fibrosis compared with vehicle-treated counterparts. Px is a U.S. Food and Drug Administration–approved compound currently prescribed as a selective serotonin reuptake inhibitor with potent efficacy on a range of cellular proteins (49). For example, off-label use has proved effective in the treatment of menopausal symptoms and responsiveness to antiestrogenic cancer therapy because of the inhibition of the cytochrome P450 family of enzymes (49). In addition, multiple studies have pointed to its efficacy as a selective GRK2 inhibitor in promoting productive repair pathways in the heart (44, 45, 50). Notably, it has been shown to inhibit GRK2 downstream of S1PR1 ligation, preventing S1PR1 phosphorylation and internalization (39). Interestingly, we observed a survival benefit with Px treatment compared with vehicle that was not observed with therapeutic induction of genetic S1PR1 overexpression, whereas both approaches were sufficient to reduce postviral fibrosis. As such, Px treatment may have multiple beneficial effects beyond GRK2 inhibition and stabilization of EC S1PR1, which contribute to the observed attenuation of postviral fibrosis. However, in support of our GRK2-centric conclusions, GRK2 inhibition with CAS 24269-96-3 has also been shown to be effective in protecting against bleomycin-induced lung fibrosis (51). The availability and *in vivo* efficacy and tolerability of Px make it an attractive translational tool for intervention during viral infection to improve outcomes, including the attenuation of postviral fibrosis. Interestingly, Px use has been found to be associated with reduced risk of intubation or death in hospitalized patients with COVID-19 (52), although further studies are needed to confirm the link to postviral fibrosis.

Despite the pulmonary endothelium playing an important role in the development of ARDS, the therapeutic potential of modulating EC signaling to prevent deleterious long-term consequences has not been well explored. Given the continuous global burden of respiratory viral infections, there is a great need for novel therapies targeted at reducing long-term postviral fibrotic complications. Currently, limited data exist regarding the efficacy of traditional antifibrotics pirfenidone and nintedanib on the resolution of postviral fibrosis. As such, new therapeutic avenues must continue to be explored (53, 54). Augmentation of S1PR1, a key protective signaling axis for the lung endothelium, has the potential to reduce the burden of postviral fibrosis. ■

Author disclosures are available with the text of this article at www.atsjournals.org.

References

1. Thompson BT, Chambers RC, Liu KD. Acute respiratory distress syndrome. *N Engl J Med* 2017;377:1904–1905.
2. Shah RD, Wunderink RG. Viral pneumonia and acute respiratory distress syndrome. *Clin Chest Med* 2017;38:113–125.
3. Shojaee A, Siner JM, Zinchuk A, Aryan Y, Kaminski N, Dela Cruz CS. Viral pneumonia is associated with increased risk and earlier development of post-inflammatory pulmonary fibrosis [preprint]. medRxiv; 2021 [accessed 2023 Nov 1]. Available from: https://doi.org/10.1101/2021.03.08.21252412.
4. Naik PK, Moore BB. Viral infection and aging as cofactors for the development of pulmonary fibrosis. *Expert Rev Respir Med* 2010;4:759–771.
5. Papazian L, Doddoli C, Chetaille B, Gernez Y, Thirion X, Roch A, *et al.* A contributive result of open-lung biopsy improves survival in acute respiratory distress syndrome patients. *Crit Care Med* 2007;35:755–762.
6. McDonald LT. Healing after COVID-19: are survivors at risk for pulmonary fibrosis? *Am J Physiol Lung Cell Mol Physiol* 2021;320:L257–L265.
7. Teuwen LA, Geldhof V, Pasut A, Carmeliet P. COVID-19: the vasculature unleashed. *Nat Rev Immunol* 2020;20:389–391.
8. Burnham EL, Janssen WJ, Riches DW, Moss M, Downey GP. The fibroproliferative response in acute respiratory distress syndrome: mechanisms and clinical significance. *Eur Respir J* 2014;43:276–285.
9. Keeler SP, Agapov EV, Hinojosa ME, Letvin AN, Wu K, Holtzman MJ. Influenza A virus infection causes chronic lung disease linked to sites of active viral RNA remnants. *J Immunol* 2018;201:2354–2368.
10. Patel SR, Karmpaliotis D, Ayas NT, Mark EJ, Wain J, Thompson BT, *et al.* The role of open-lung biopsy in ARDS. *Chest* 2004;125:197–202.
11. Qiao J, Zhang M, Bi J, Wang X, Deng G, He G, *et al.* Pulmonary fibrosis induced by H5N1 viral infection in mice. *Respir Res* 2009;10:107.
12. Maniatis NA, Orfanos SE. The endothelium in acute lung injury/acute respiratory distress syndrome. *Curr Opin Crit Care* 2008;14:22–30.
13. Millar FR, Summers C, Griffiths MJ, Toshner MR, Proudfoot AG. The pulmonary endothelium in acute respiratory distress syndrome: insights and therapeutic opportunities. *Thorax* 2016;71:462–473.
14. Knipe RS, Spinney JJ, Abe EA, Probst CK, Franklin A, Logue A, *et al.* Endothelial-specific loss of sphingosine-1-phosphate receptor 1 increases vascular permeability and exacerbates bleomycin-induced pulmonary fibrosis. *Am J Respir Cell Mol Biol* 2022;66:38–52.
15. Probst CK, Montesi SB, Medoff BD, Shea BS, Knipe RS. Vascular permeability in the fibrotic lung. *Eur Respir J* 2020;56:1900100.
16. Teijaro JR, Walsh KB, Cahalan S, Fremgen DM, Roberts E, Scott F, *et al.* Endothelial cells are central orchestrators of cytokine amplification during influenza virus infection. *Cell* 2011;146:980–991.
17. Zhang K, Wang P, Huang S, Wang X, Li T, Jin Y, *et al.* Different mechanism of LPS-induced calcium increase in human lung epithelial cell and microvascular endothelial cell: a cell culture study in a model for ARDS. *Mol Biol Rep* 2014;41:4253–4259.
18. Bachofen M, Weibel ER. Alterations of the gas exchange apparatus in adult respiratory insufficiency associated with septicemia. *Am Rev Respir Dis* 1977;116:589–615.
19. Radomski MW, Palmer RM, Moncada S. Endogenous nitric oxide inhibits human platelet adhesion to vascular endothelium. *Lancet* 1987;2:1057–1058.
20. Nuckton TJ, Alonso JA, Kallet RH, Daniel BM, Pittet JF, Eisner MD, *et al.* Pulmonary dead-space fraction as a risk factor for death in the acute respiratory distress syndrome. *N Engl J Med* 2002;346:1281–1286.

21. Yanagihara T, Tsubouchi K, Gholiof M, Chong SG, Lipson KE, Zhou Q, *et al.* Connective-tissue growth factor (CTGF/CCN2) contributes to TGF-β1-induced lung fibrosis. *Am J Respir Cell Mol Biol* 2022;66: 260–270.
22. Synenki L, Chandel NS, Budinger GR, Donnelly HK, Topin J, Eisenbart J, *et al.* Bronchoalveolar lavage fluid from patients with acute lung injury/acute respiratory distress syndrome induces myofibroblast differentiation. *Crit Care Med* 2007;35:842–848.
23. Oo ML, Chang SH, Thangada S, Wu MT, Rezaul K, Blaho V, *et al.* Engagement of $S1P_1$-degradative mechanisms leads to vascular leak in mice. *J Clin Invest* 2011;121:2290–2300.
24. Shea BS, Brooks SF, Fontaine BA, Chun J, Luster AD, Tager AM. Prolonged exposure to sphingosine 1-phosphate receptor-1 agonists exacerbates vascular leak, fibrosis, and mortality after lung injury. *Am J Respir Cell Mol Biol* 2010;43:662–673.
25. Choi JW, Gardell SE, Herr DR, Rivera R, Lee CW, Noguchi K, *et al.* FTY720 (fingolimod) efficacy in an animal model of multiple sclerosis requires astrocyte sphingosine 1-phosphate receptor 1 (S1P1) modulation. *Proc Natl Acad Sci USA* 2011;108:751–756.
26. Shi X, Wang W, Li J, Wang T, Lin Y, Huang S, *et al.* Sphingosine 1-phosphate receptor 1 regulates cell-surface localization of membrane proteins in endothelial cells. *Biochim Biophys Acta Gen Subj* 2019; 1863:1079–1087.
27. Pitulescu ME, Schmidt I, Benedito R, Adams RH. Inducible gene targeting in the neonatal vasculature and analysis of retinal angiogenesis in mice. *Nat Protoc* 2010;5:1518–1534.
28. Cho JL, Roche MI, Sandall B, Brass AL, Seed B, Xavier RJ, *et al.* Enhanced Tim3 activity improves survival after influenza infection. *J Immunol* 2012;189:2879–2889.
29. Glenn JD, Smith MD, Xue P, Chan-Li Y, Collins S, Calabresi PA, *et al.* CNS-targeted autoimmunity leads to increased influenza mortality in mice. *J Exp Med* 2017;214:297–307.
30. Moltedo B, Li W, Yount JS, Moran TM. Unique type I interferon responses determine the functional fate of migratory lung dendritic cells during influenza virus infection. *PLoS Pathog* 2011;7:e1002345.
31. Langouët-Astrié C, Oshima K, McMurtry SA, Yang Y, Kwiecinski JM, LaRivière WB, *et al.* The influenza-injured lung microenvironment promotes MRSA virulence, contributing to severe secondary bacterial pneumonia. *Cell Rep* 2022;41:111721.
32. Brazee PL, Morales-Nebreda L, Magnani ND, Garcia JG, Misharin AV, Ridge KM, *et al.* Linear ubiquitin assembly complex regulates lung epithelial-driven responses during influenza infection. *J Clin Invest* 2020;130:1301–1314.
33. Ashcroft T, Simpson JM, Timbrell V. Simple method of estimating severity of pulmonary fibrosis on a numerical scale. *J Clin Pathol* 1988;41: 467–470.
34. Frej C, Andersson A, Larsson B, Guo LJ, Norström E, Happonen KE, *et al.* Quantification of sphingosine 1-phosphate by validated LC-MS/MS method revealing strong correlation with apolipoprotein M in plasma but not in serum due to platelet activation during blood coagulation. *Anal Bioanal Chem* 2015;407:8533–8542.
35 El Refaey H, Al Amri HS, Ashour AE, Ahmed AF. Administration of zinc with paroxetine improved the forced swim test behavioral pattern of treated mice in acute and sub-acute study. *J Behav Brain Sci* 2015;05: 57773.
36. Kantor S, Varga J, Kulkarni S, Morton AJ. Chronic paroxetine treatment prevents the emergence of abnormal electroencephalogram oscillations in Huntington's disease mice. *Neurotherapeutics* 2017;14:1120–1133.
37. Coleman FH, Christensen HD, Gonzalez CL, Rayburn WF. Behavioral changes in developing mice after prenatal exposure to paroxetine (Paxil). *Am J Obstet Gynecol* 1999;181:1166–1171.
38. Shea BS, Probst CK, Brazee PL, Rotile NJ, Blasi F, Weinreb PH, *et al.* Uncoupling of the profibrotic and hemostatic effects of thrombin in lung fibrosis. *JCI Insight* 2017;2:e86608.
39. Martínez-Morales JC, Romero-Ávila MT, Reyes-Cruz G, García-Sáinz JA. $S1P_1$ receptor phosphorylation, internalization, and interaction with Rab proteins: effects of sphingosine 1-phosphate, FTY720-P, phorbol esters, and paroxetine. *Biosci Rep* 2018;38:BSR20181612.
40. Gonzalez-Cabrera PJ, Jo E, Sanna MG, Brown S, Leaf N, Marsolais D, *et al.* Full pharmacological efficacy of a novel S1P1 agonist that does not require S1P-like headgroup interactions. *Mol Pharmacol* 2008;74: 1308–1318.
41. Gatfield J, Monnier L, Studer R, Bolli MH, Steiner B, Nayler O. Sphingosine-1-phosphate (S1P) displays sustained S1P1 receptor agonism and signaling through S1P lyase-dependent receptor recycling. *Cell Signal* 2014;26:1576–1588.
42. Cartier A, Hla T. Sphingosine 1-phosphate: lipid signaling in pathology and therapy. *Science* 2019;366:eaar5551.
43. Huang LS, Sudhadevi T, Fu P, Punathil-Kannan PK, Ebenezer DL, Ramchandran R, *et al.* Sphingosine kinase 1/S1P signaling contributes to pulmonary fibrosis by activating Hippo/YAP pathway and mitochondrial reactive oxygen species in lung fibroblasts. *Int J Mol Sci* 2020;21:2064.
44. Schumacher SM, Gao E, Zhu W, Chen X, Chuprun JK, Feldman AM, *et al.* Paroxetine-mediated GRK2 inhibition reverses cardiac dysfunction and remodeling after myocardial infarction. *Sci Transl Med* 2015;7:277ra31.
45. Sun X, Zhou M, Wen G, Huang Y, Wu J, Peng L, *et al.* Paroxetine attenuates cardiac hypertrophy via blocking GRK2 and ADRB1 interaction in hypertension. *J Am Heart Assoc* 2021;10:e016364.
46. Bu Y, Wu H, Deng R, Wang Y. Therapeutic potential of SphK1 inhibitors based on abnormal expression of SphK1 in inflammatory immune related-diseases. *Front Pharmacol* 2021;12:733387.
47. Gowda D, Ohno M, B Gowda SG, Chiba H, Shingai M, Kida H, *et al.* Defining the kinetic effects of infection with influenza virus A/PR8/34 (H1N1) on sphingosine-1-phosphate signaling in mice by targeted LC/MS. *Sci Rep* 2021;11:20161.
48. Kim S, Bielawski J, Yang H, Kong Y, Zhou B, Li J. Functional antagonism of sphingosine-1-phosphate receptor 1 prevents cuprizone-induced demyelination. *Glia* 2018;66:654–669.
49. Kowalska M, Nowaczyk J, Fijałkowski Ł, Nowaczyk A. Paroxetine—overview of the molecular mechanisms of action. *Int J Mol Sci* 2021;22: 1662.
50. Lassen TR, Nielsen JM, Johnsen J, Ringgaard S, Bøtker HE, Kristiansen SB. Effect of paroxetine on left ventricular remodeling in an in vivo rat model of myocardial infarction. *Basic Res Cardiol* 2017;112:26.
51. Li Y, Sun Y, Wu N, Ma H. GRK2 promotes activation of lung fibroblast cells and contributes to pathogenesis of pulmonary fibrosis through increasing Smad3 expression. *Am J Physiol Cell Physiol* 2022;322: C63–C72.
52. Hoertel N, Sánchez-Rico M, Vernet R, Beeker N, Jannot AS, Neuraz A, *et al.*; AP-HP/Universities / INSERM COVID-19 Research Collaboration and AP-HP COVID CDR Initiative. Association between antidepressant use and reduced risk of intubation or death in hospitalized patients with COVID-19: results from an observational study. *Mol Psychiatry* 2021; 26:5199–5212.
53. Choudhary R, Kumar A, Ali O, Pervez A. Effectiveness and safety of pirfenidone and nintedanib for pulmonary fibrosis in COVID-19-induced severe pneumonia: an interventional study. *Cureus* 2022;14:e29435.
54. Saiphoklang N, Patanayindee P, Ruchiwit P. The effect of nintedanib in post-COVID-19 lung fibrosis: an observational study. *Crit Care Res Pract* 2022;2022:9972846.